Optimal thrust control with magnitude and direction constraints

Optimal Thrust Control with Magnitude and Direction Constraints

Hong-Xin Shen[a], Zhi-Sheng Duan[b], Lorenzo Casalino[c,*]

[a] *Peking University, Department of Mechanics and Engineering Science, College of Engineering, 5 Yiheyuan Road, Haidian District, 100871 Beijing, China*
[b] *Peking University, Department of Mechanics and Engineering Science, College of Engineering, 5 Yiheyuan Road, Haidian District, 100871 Beijing, China*
[c] *Politecnico di Torino, Department of Mechanical and Aerospace Engineering, Corso Duca degli Abruzzi, 24, Torino, 10129, Italy*

Abstract

An indirect optimization procedure is presented to minimize the propellant consumption for finite-burn transfers with two practical thrust control models, namely, inertially fixed thrust and fixed-plane linearly varying thrust direction. The optimality equations are derived with theory of optimal control and the consequent boundary value problem is solved with a procedure based on Newton's method. A homotopic approach is used to find suitable tentative solutions and assure convergence. The method is applied to the optimization of Moon escape trajectories with accurate dynamic models and proves to be fast and accurate.

Keywords: Indirect optimization methods, Finite thrust, Chemical propulsion, Thrust direction constraints

1. Introduction

An indirect optimization procedure is presented to optimize the fuel usage for finite-burn transfers with practical thrust controls. In the mission design of finite-burn transfers, impulsive approximation is often used. Once the impulsive solutions are obtained, the impulses are converted to finite burns with inertially fixed thrust directions. Although it is valid for high enough thrust-to-mass ratio, a more realistic finite-burn solution is required when the thrust arc length is not negligible; these situations often happen when the thrust magnitude is modest while the required velocity change is significant. Also, in mission design it is generally assumed that the thrust direction can be adjusted freely without constraining the thrust steering rate, which however is not practical to carry out because of the capability limitations of reaction control system.

*Corresponding author
Email addresses: hongxin.shen@gmail.com (Hong-Xin Shen), duanzs@pku.edu.cn (Zhi-Sheng Duan), lorenzo.casalino@polito.it (Lorenzo Casalino)

The goal of this research is to develop a realistic optimal control strategy. Motivated by this desire, two realistic thrust models are taken into account. The first finite-burn model holds the thrust vector inertially fixed for each maneuver. The second finite-burn model, referred to as the fixed-plane linearly steered finite-burn model, allows the thrust vector to vary linearly in direction but constrains it to be normal to a fixed rotation axis, for each finite-burn maneuver. The latter model offers an improvement over the inertially fixed model while still remaining simple and practical for spacecraft applications. This paper extends the analysis of Ocampo and Muthur [1], who have used a direct method to optimize finite-burn trajectories with the same engine models. In contrast to past research, the current research focuses on indirect optimization and aims to avoid using analytical simplifications to the problem dynamics. The purpose is to produce a faster and more accurate indirect optimization software (in comparison to existing methods) for the analysis of complex problems with practical limitations on thrust direction and its rate of change.

The indirect method and realistic thrust models are applied to the optimization of Moon escape trajectories with accurate dynamic models. The existing typical works may simplify the dynamics for this kind of problems using two-body models [1, 3, 2, 4], the circular restricted three-body model [5], and the asymptotic expansion [6], and thus can only provide an approximate analysis as the initial guess, due to the lack of fidelity. Using the high-accuracy dynamic model, Yan et al. [7] and Park [8] optimized the three-burn Moon escape trajectories using pseudospectral methods, and an intermediate thrust arc (singular arc) was included in their optimal solutions. However, in a previous work, the authors of the present paper showed that a bang-bang control structure without singular arcs satisfies the necessary condition of optimality accurately and performs better in terms of fuel consumption [9].

Since indirect methods are based on optimal control theory, they are intrinsically fast and accurate [10]. An indirect optimization procedure is presented here to obtain the necessary conditions of optimality associated with the practical thrust models, and then analyze the finite-burn Moon-escape trajectory using practical thrust as well as accurate dynamic models. Specific strategies based on homotopy/smoothing must be employed to obtain convergence, such as the methods proposed in Refs. [11, 12, 13, 15, 14, 16]. Optimal impulsive solutions and freely steering finite-burn solutions for the problem are here found with procedures developed by the authors and described in previous works [5, 9]. In the present work, the previous solutions are in turn used as starting guess for the finite-thrust problem with practical thrust models and no convergence difficulties are experienced. This work extends the techniques previously developed and justifies the effectiveness of the indirect method in producing optimal and accurate solutions for complex as well as realistic optimization problems.

2. Problem Statement

Here we consider the spacecraft trajectory subject to the gravitational effects of multiple bodies, whose positions relative to the central body are obtained from

the JPL DE405 ephemeris. This work adopts J2000 Cartesian coordinates, in which the system state dynamics $\boldsymbol{f}^T = [\dot{x}\ \dot{y}\ \dot{z}\ \dot{v}_x\ \dot{v}_y\ \dot{v}_z\ \dot{m}]$ is written as:

$$\dot{x} = v_x \tag{1}$$

$$\dot{y} = v_y \tag{2}$$

$$\dot{z} = v_z \tag{3}$$

$$\dot{v}_x = -\frac{\mu_c x}{r_c^3} - \sum_{k=1}^{N}\left[\frac{\mu_{p_k}(x - x_{p_k})}{R_{p_k}^3} + \frac{\mu_{p_k} x_{p_k}}{r_{p_k}^3}\right] + \frac{T_x}{m} \tag{4}$$

$$\dot{v}_y = -\frac{\mu_c y}{r_c^3} - \sum_{k=1}^{N}\left[\frac{\mu_{p_k}(y - y_{p_k})}{R_{p_k}^3} + \frac{\mu_{p_k} y_{p_k}}{r_{p_k}^3}\right] + \frac{T_y}{m} \tag{5}$$

$$\dot{v}_z = -\frac{\mu_c z}{r_c^3} - \sum_{k=1}^{N}\left[\frac{\mu_{p_k}(z - z_{p_k})}{R_{p_k}^3} + \frac{\mu_{p_k} z_{p_k}}{r_{p_k}^3}\right] + \frac{T_z}{m} \tag{6}$$

$$\dot{m} = -\frac{T}{c} \tag{7}$$

where T is the engine thrust and $c = g_0 I_{sp}$ is the exhaust velocity (which is proportional to the specific impulse I_{sp} and the standard acceleration of gravity at sea level $g_0 = 9.80665\,\mathrm{m/s^2}$). The gravitational parameters of the central body and the generic k-th perturbing body are denoted by μ_c and μ_{p_k}, respectively. The distance between the spacecraft and the central body is $r = \sqrt{x^2 + y^2 + z^2}$; the spacecraft distance from the perturbing body is $R_{p_k} = \sqrt{(x - x_{p_k})^2 + (y - y_{p_k})^2 + (z - z_{p_k})^2}$. The time-varying components of the perturbing body position vector, with respect to the instantaneous center of the central body, are denoted as $(x_{p_k}, y_{p_k}, z_{p_k})$, and they are directly obtained as functions of time from JPL DE405 ephemeris. As a consequence, Eqs. (4)-(6) are non-autonomous. Finally, $r_{p_k} = \sqrt{x_{p_k}^2 + y_{p_k}^2 + z_{p_k}^2}$ represents the distance of the perturbing body with respect to the instantaneous center of the central body. In order to improve numerical accuracy, variables are made nondimensional by using the radius and gravity constant of the central body as reference values. However, results are presented in dimensional form for a more direct interpretation. The thrust components T_x, T_y, and T_z are expressed as function of azimuth and elevation angles of the thrust vector, α and β, respectively, which are defined in spherical coordinates, with $\alpha \in [0, 2\pi]$ and $\beta \in [-\pi/2, \pi/2]$:

$$T_x = \cos\alpha\cos\beta,\ T_y = \sin\alpha\cos\beta,\ T_z = \sin\beta \tag{8}$$

Thrust T may be freely or restrictively controlled in practical ways as described in the following section.

To minimize the propellant consumption, the final mass is maximized given the initial mass; therefore, the performance index is

$$\varphi = m(t_f) \tag{9}$$

The mission is specified by assigning initial and target conditions in terms of position and velocity, in a limited flight time span.

3. Practical Finite-Thrust Models

3.1. Inertially Fixed Thrust Model

The thrust vector along the finite-burn arc is assumed inertially fixed. During the j-th burn ($j = 1, ..., f$), the thrust angles remain fixed in the inertial frame at α_j and β_j, and the thrust components are

$$T_x = T\cos\alpha_j\cos\beta_j,\ T_y = T\sin\alpha_j\cos\beta_j,\ T_z = T\sin\beta_j \tag{10}$$

The control angles α and β are considered as additional piecewise-constant state variables with trivial state equations

$$\dot{\alpha} = 0,\ \dot{\beta} = 0 \tag{11}$$

3.2. Fixed-Plane Linearly Varying Thrust Model

This case assumes that the thrust direction rotates at a constant rate in a fixed plane, which is defined by a fixed rotation axis, during each finite-burn maneuver. The thrust magnitude remains constant, and the fixed rotation axis and rotation rate are optimization variables for each finite-burn arc. A unit vector $\boldsymbol{J}$ is defined, orthogonal to the fixed plane in which the thrust direction $\boldsymbol{u}$ rotates at a constant rate ω. The relevant vectors to determine the thrust direction are represented in Figure 1. The vector $\boldsymbol{J}$ can be defined as

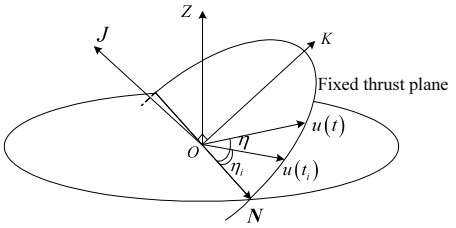

Figure 1: Fixed-plane linearly steered finite-burn model, showing the fixed rotation plane and steering parameters.

$$\boldsymbol{J} = [\cos\alpha_J\cos\delta_J \quad \sin\alpha_J\cos\delta_J \quad \sin\delta_J]^T \tag{12}$$

where α_J and δ_J are the azimuth and elevation angles of $\boldsymbol{J}$ vector, respectively, with respect to the reference plane. The ascending node direction between thrust plane and equatorial plane is denoted as $\boldsymbol{N}$, which is

$$\boldsymbol{N} = \boldsymbol{Z} \times \boldsymbol{J} = [-\sin\alpha_J \quad \cos\alpha_J \quad 0]^T \tag{13}$$

$\boldsymbol{K}$ is defined in the thrust plane, orthogonal to $\boldsymbol{N}$

$$\boldsymbol{K} = \boldsymbol{J} \times \boldsymbol{N} = [-\cos\alpha_J\sin\delta_J \quad -\sin\alpha_J\sin\delta_J \quad \cos\delta_J]^T \tag{14}$$

Hence, the thrust direction $\boldsymbol{u}$ can be defined at a given time t:

$$\boldsymbol{u}(t) = \cos\eta(t)\boldsymbol{N} + \sin\eta(t)\boldsymbol{K} \tag{15}$$

$$\eta(t) = \eta(t_i) + \omega(t - t_i) \tag{16}$$

where t_i represents the initial time of a thrust arc. For brevity, $\eta(t)$ and $\eta(t_i)$ are simply denoted η and η_i instead. The augmented variables to be optimized for this model are α_J, δ_J, η_i, and ω, with trivial state equations:

$$\dot{\alpha}_J = 0,\ \dot{\delta}_J = 0,\ \dot{\eta}_i = 0,\ \dot{\omega} = 0 \tag{17}$$

4. Optimal Control

The performance index φ, which is given by Eq. (9), is maximized by applying the theory of optimal control [17, 18]. Adjoint variables are introduced $\boldsymbol{\lambda}^T = [\lambda_x \lambda_y \lambda_z \lambda_{v_x} \lambda_{v_y} \lambda_{v_z} \lambda_m]$ to define the Hamiltonian function $H = \boldsymbol{\lambda}^T \boldsymbol{f}$, where $\boldsymbol{f}$ is the state differential equation vector, consisting of the right-hand sides of Eqs. (1)-(7). The adjoint dynamics can be readily derived through the Euler-Lagrange equations:

$$\dot{\lambda}_x = \lambda_{v_x} \tfrac{\mu_c}{r_c^3} - \tfrac{3\mu_c}{r_c^5} x(\lambda_{v_x} x + \lambda_{v_y} y + \lambda_{v_z} z) + \Delta\dot{\lambda}_{px} \tag{18}$$

$$\dot{\lambda}_y = \lambda_{v_y} \tfrac{\mu_c}{r_c^3} - \tfrac{3\mu_c}{r_c^5} y(\lambda_{v_x} x + \lambda_{v_y} y + \lambda_{v_z} z) + \Delta\dot{\lambda}_{py} \tag{19}$$

$$\dot{\lambda}_z = \lambda_{v_z} \tfrac{\mu_c}{r_c^3} - \tfrac{3\mu_c}{r_c^5} z(\lambda_{v_x} x + \lambda_{v_y} y + \lambda_{v_z} z) + \Delta\dot{\lambda}_{pz} \tag{20}$$

$$\dot{\lambda}_{v_x} = -\lambda_x \tag{21}$$

$$\dot{\lambda}_{v_y} = -\lambda_y \tag{22}$$

$$\dot{\lambda}_{v_z} = -\lambda_z \tag{23}$$

$$\dot{\lambda}_m = \frac{T \left\| \boldsymbol{\lambda}_V \right\|}{m^2} \tag{24}$$

where the velocity adjoint vector $\boldsymbol{\lambda}_V = [\lambda_{v_x} \lambda_{v_y} \lambda_{v_z}]^T$, i.e., the primer vector [19], has been introduced. The sum of the contributions of the perturbations $\Delta\dot{\lambda}_{px}$, $\Delta\dot{\lambda}_{px}$, and $\Delta\dot{\lambda}_{pz}$ are easily derived

$$\begin{aligned} \Delta\dot{\lambda}_{px} = & -\sum_{k=1}^{N} \left\{ \lambda_{v_x} \left[-\frac{\mu_{p_k}}{R_{p_k}^3} + \frac{3\mu_{p_k}}{R_{p_k}^5} (x - x_{p_k})^2 \right] \right. \\ & \left. + \lambda_{v_y} \left[\frac{3\mu_{p_k}}{R_{p_k}^5} (x - x_{p_k})(y - y_{p_k}) \right] + \lambda_{v_z} \left[\frac{3\mu_{p_k}}{R_{p_k}^5} (x - x_{p_k})(z - z_{p_k}) \right] \right\} \end{aligned} \tag{25}$$

$$\begin{aligned} \Delta\dot{\lambda}_{py} = & -\sum_{k=1}^{N} \left\{ \lambda_{v_y} \left[-\frac{\mu_{p_k}}{R_{p_k}^3} + \frac{3\mu_{p_k}}{R_{p_k}^5} (y - y_{p_k})^2 \right] \right. \\ & \left. + \lambda_{v_x} \left[\frac{3\mu_{p_k}}{R_{p_k}^5} (x - x_{p_k})(y - y_{p_k}) \right] + \lambda_{v_z} \left[\frac{3\mu_{p_k}}{R_{p_k}^5} (y - y_{p_k})(z - z_{p_k}) \right] \right\} \end{aligned} \tag{26}$$

$$\begin{aligned} \Delta\dot{\lambda}_{pz} = & -\sum_{k=1}^{N} \left\{ \lambda_{v_z} \left[-\frac{\mu_{p_k}}{R_{p_k}^3} + \frac{3\mu_{p_k}}{R_{p_k}^5} (z - z_{p_k})^2 \right] \right. \\ & \left. + \lambda_{v_y} \left[\frac{3\mu_{p_k}}{R_{p_k}^5} (y - y_{p_k})(z - z_{p_k}) \right] + \lambda_{v_x} \left[\frac{3\mu_{p_k}}{R_{p_k}^5} (x - x_{p_k})(z - z_{p_k}) \right] \right\} \end{aligned} \tag{27}$$

The thrust direction and magnitude are the problem control variables, which must maximize H in agreement with Pontryagin's Maximum Principle (PMP).

For a freely-steering spacecraft, in the absence of constraints, the optimal thrust direction must be parallel to the primer vector $\boldsymbol{\lambda}_V$, that is,

$$T_x = \frac{\lambda_{v_x}}{\|\boldsymbol{\lambda}_V\|},\ T_y = \frac{\lambda_{v_y}}{\|\boldsymbol{\lambda}_V\|},\ T_z = \frac{\lambda_{v_z}}{\|\boldsymbol{\lambda}_V\|} \tag{28}$$

and, the thrust multiplier, i.e., the switching function, becomes

$$S_F = \|\boldsymbol{\lambda}_V\| / m - \lambda_m / c \tag{29}$$

The Hamiltonian is linear with respect to the thrust magnitude; H is maximized by the maximum value of the thrust magnitude if the switching function S_F is positive, whereas T must be set to zero when S_F is negative. This bang-bang control (when S_F is null only at a finite number of points) is usually the optimal strategy for the thrust magnitude control in aerospace problems, where T appears linearly in the Hamiltonian. Singular arc solutions may exist when S_F is null over a time interval and intermediate thrust is instead used. Bang-bang control is first assumed, but the switching function must be checked carefully a posteriori for anomalies in the switching function behavior, which may suggest the presence of singular arcs [20].

The number and order of the arcs, which define the trajectory switching structure, must be preliminarily assumed. The optimal solution that corresponds to the assigned switching structure is then checked in the light of PMP. If PMP is violated, the behavior of the S_F suggests a different switching structure, with the addition/removal of thrust/coast arcs, and an improved solution is obtained when the correct optimal structure is found. In this formulation, the arc time-lengths are additional unknowns and are implicitly determined by the optimality conditions. These conditions state that the switching function must be null at the extremities of each thrust arc, that is $S_{F_j} = 0,\ j = 1, 2, ..., f-1$. Due to homogeneous property in the adjoint variables, one can replace the optimality condition $\lambda_{m_f} = 1$ with $\lambda_{m_0} = 1$, thus reducing the number of unknowns.

When considering the practical thrust control models, as presented in Section3, new necessary optimality necessary conditions, which will be presented in the following section, should be derived according to the PMP.

4.1. Inertially Fixed Thrust

Thrust azimuth and elevation angles are treated as additional state variables with trivial state equations $\dot{\alpha} = 0$, $\dot{\beta} = 0$. Two adjoint variables λ_α and λ_β are introduced, with associated Euler-Lagrange equations

$$\dot{\lambda}_\alpha = -\frac{T}{m}\left(-\lambda_{v_x}\sin\alpha\cos\beta + \lambda_{v_y}\cos\alpha\cos\beta\right) \tag{30}$$

$$\dot{\lambda}_\beta = -\frac{T}{m}\left(-\lambda_{v_x}\cos\alpha\sin\beta - \lambda_{v_y}\sin\alpha\sin\beta + \lambda_{v_z}\cos\beta\right) \tag{31}$$

The switching function becomes

$$S_F = \left(\lambda_{v_x}\cos\alpha\cos\beta + \lambda_{v_y}\sin\alpha\cos\beta + \lambda_{v_z}\sin\beta\right)/m - \lambda_m/c \tag{32}$$

and replaces Eq.(29). Also, the differential equation for λ_m, i.e., Eq. (24), should be updated

$$\dot{\lambda}_m = \frac{T}{m^2}\left(\lambda_{v_x}\cos\alpha\cos\beta + \lambda_{v_y}\sin\alpha\cos\beta + \lambda_{v_z}\sin\beta\right) \tag{33}$$

The optimal control theory is applied to determine the optimal thrust directions. The thrust angles do not explicitly appear in the boundary conditions and therefore the optimality conditions are

$$\lambda_{\alpha_j} = 0,\ j = 1, ..., f \tag{34}$$

$$\lambda_{\beta_j} = 0,\ j = 1, ..., f \tag{35}$$

One should note that λ_α and λ_β are null during all coast arcs, where α and β have no meaning. The four boundary conditions at the extremities of each thrust arc determine the values of the additional adjoint variables at the start of the arc (explicitly) and the values of α and β (implicitly).

4.2. Fixed-Plane Linearly Varying Thrust

Accordingly, the augmented Euler-Lagrange equations are

$$\dot{\lambda}_{\alpha_J} = -\frac{T}{m}\left(-\lambda_{v_x}A_x + \lambda_{v_y}A_y + \lambda_{v_y}A_z\right) \tag{36}$$

$$\dot{\lambda}_{\delta_J} = -\frac{T}{m}\left(-\lambda_{v_x}B_x + \lambda_{v_y}B_y + \lambda_{v_y}B_z\right) \tag{37}$$

$$\dot{\lambda}_{\eta_i} = -\frac{T}{m}\left(-\lambda_{v_x}C_x + \lambda_{v_y}C_y + \lambda_{v_y}C_z\right) \tag{38}$$

$$\dot{\lambda}_{\omega} = -\frac{T}{m}\left(-\lambda_{v_x}D_x + \lambda_{v_y}D_y + \lambda_{v_y}D_z\right) \tag{39}$$

$$A_x = -\cos\eta\cos\alpha_J + \sin\eta\sin\alpha_J\sin\delta_J \tag{40}$$

$$A_y = -\cos\eta\sin\alpha_J - \sin\eta\cos\alpha_J\sin\delta_J \tag{41}$$

$$A_z = 0 \tag{42}$$

$$B_x = -\sin\eta\cos\alpha_J\cos\delta_J \tag{43}$$

$$B_y = -\sin\eta\sin\alpha_J\cos\delta_J \tag{44}$$

$$B_z = -\sin\eta\sin\alpha_J \tag{45}$$

$$C_x = \sin\eta\sin\alpha_J - \cos\eta\cos\alpha_J\sin\delta_J \tag{46}$$

$$C_y = -\sin\eta\cos\alpha_J - \cos\eta\sin\alpha_J\sin\delta_J \tag{47}$$

$$C_z = \cos\eta\cos\alpha_J \tag{48}$$

$$D_x = C_x(t - t_i) \tag{49}$$

$$D_y = C_y(t - t_i) \tag{50}$$

$$D_z = C_z(t - t_i) \tag{51}$$

In similarity to the previous model, the augmented adjoints at the bound of each burn arc are null

$$\lambda_{\alpha_{Jj}} = 0,\ j = 1, ..., f \tag{52}$$

$$\lambda_{\delta_{Jj}} = 0,\ j = 1, ..., f \tag{53}$$

$$\lambda_{\eta_{ij}} = 0,\ j = 1, ..., f \tag{54}$$

$$\lambda_{\omega_j} = 0,\ j = 1, ..., f \tag{55}$$

The switching function and differential equation of mass adjoint, which are similar to those of the first model, are also in general form

$$S_F = \left(\lambda_{v_x} u_x + \lambda_{v_y} u_y + \lambda_{v_z} u_z\right)/m - \lambda_m/c \tag{56}$$

$$\dot{\lambda}_m = \frac{T}{m^2}\left(\lambda_{v_x} u_x + \lambda_{v_y} u_y + \lambda_{v_z} u_z\right) \tag{57}$$

The corresponding boundary conditions have been determined, and hence the optimal control problem has been converted into a multi-point boundary value problem (MPBVP). Provided a tentative solution is given, the tentative values are then iteratively corrected to fulfill the boundary conditions. An impulsive solution is first sought; a homotopic approach [21, 5] was developed to find optimal impulsive solutions starting from a generic guess, and is here profitably employed. Then, impulses are replaced by finite burn arcs and the thrust is gradually reduced to achieve the required finite-burn solution with free thrust direction; the impulsive solution can be used to estimate the burn durations (from ΔV, mass, and thrust level) and thus the engine switching times, which are problem unknowns, in addition to the adjoint variables. In the specific cases treated here, solutions with the Orion main engine can be directly obtained by using the impulsive solutions as tentative value, as the thrust level is quite large; Two intermediate levels between the Orion main and auxiliary engine thrust values (e.g. 20 kN and 10 kN) allow one to move from Case 1 to Case 2 solutions. Finally, the free-steering solution is used as tentative guess to find the optimal solution for the practical thrust models described above. A classic shooting procedure [22] based on Newton's method is used for the solution of the resulting MPBVP in each step.

5. Application to Lunar Escape Trajectories

Initial conditions place the spacecraft on a circular orbit around the Moon; final conditions fix a desired hyperbolic escape state, through which the spacecraft transfers to a desired Earth interface condition that is designed for Earth reentry. A maximum time of flight of 48 hours is imposed, like, e.g., in the case of emergency reentry. The final mass is maximized, that is, the propellant mass is minimized. The central body is the Moon, and the perturbing bodies include the Earth and Sun, whose precise positions are computed based on JPL

ephemeris. This paper uses previous published works of Ref. [7, 8, 9] as a benchmarking resource. The initial state is given in the J2000 Moon-centered frame at a 100 km-altitude low lunar orbit (epoch 4 April 2024 15:30:00 TDT):

$$\boldsymbol{r}\left(t_0\right) = \begin{bmatrix} -1.2368 \times 10^3\,\mathrm{km} \\ 1.2681 \times 10^3\,\mathrm{km} \\ 4.6838 \times 10^2\,\mathrm{km} \end{bmatrix}, \qquad \boldsymbol{v}\left(t_0\right) = \begin{bmatrix} 3.2911 \times 10^{-2}\,\mathrm{km/s} \\ 5.8927 \times 10^{-1}\,\mathrm{km/s} \\ -1.5281 \times 10^0\,\mathrm{km/s} \end{bmatrix} \tag{58}$$

The terminal conditions are defined by a specified position and velocity vector also in the J2000 Moon-centered inertial frame:

$$\boldsymbol{r}\left(t_f\right) = \begin{bmatrix} 2.1052 \times 10^3\,\mathrm{km} \\ 3.5932 \times 10^3\,\mathrm{km} \\ 6.0825 \times 10^2\,\mathrm{km} \end{bmatrix}, \qquad \boldsymbol{v}\left(t_f\right) = \begin{bmatrix} -1.5103 \times 10^{-1}\,\mathrm{km/s} \\ -3.2129 \times 10^{-1}\,\mathrm{km/s} \\ -1.7944 \times 10^0\,\mathrm{km/s} \end{bmatrix} \tag{59}$$

It is worth noting that the final state vector used here has been slightly adjusted to fit entry interface conditions better, so they are a little different from the values used in previous research[7, 8, 9]. The spacecraft total mass (20339.9 kg) and fuel mass (8063.65 kg) are specified, and the flight time is limited to $t_f - t_0 \leq 2$ days.

Two kinds of engines with different assigned values of thrust and specific impulse are considered: 1) Main engine of the Orion spacecraft with thrust: 33361.6621 N, specific impulse: 326 s; 2) auxiliary engine of the Orion spacecraft with thrust: 4448 N, specific impulse: 309 s. These two engines replicate the conditions of the transfer example [7] using the two realistic finite-burn steering models presented here. Since the thrust-to-mass ratio of the auxiliary engine is much lower than that of the main engine, it is expected that the fixed-plane linear steering thrust model will provide a large benefit over the inertially fixed thrust steering model for the auxiliary engine.

5.1. Case 1: main engine of the Orion

The first example uses the Orion main engine, both the inertially fixed model and the linear varying model are considered. A time-free solution is first sought but the optimal flight time exceeds the 48-hour limit for the cases treated here; therefore, the equality constraint $t_f - t_0 = 2$ days is enforced. The case with inertially fixed steering is discussed as an example. The optimal solution has 3 burn arcs and four coast arcs, for a total of 19 unknowns: the time length of the coast arcs τ_{ci} $(i = 1, \ldots 4)$, the time length of the burn arcs τ_{bj} $(j = 1, \ldots 3)$, the corresponding thrust angles α_j, β_j $(j = 1, \ldots 3)$ and the initial values of the adjoint variables (except λ_{m0} set arbitrarily to 1). Unknown values of the optimal solution, made nondimensional by using the Earth-Moon system canonical units, are shown in Table 1.

Table 2 lists the fuel consumption for different steering models. When thrust direction can vary freely, the fuel consumptions of the optimal trajectory for the first, second, and third burn are 3538.05, 1257.29, and 1837.31 kg, respectively, with the total fuel consumption 6632.65 kg. For an inertially fixed thrust model, the fuel consumption for the first, second, and third burn are 3544.38, 1256.75,

Table 1: Nondimensional initial values for Case 1.

$\tau_{c1} = 1.50704335264591$	$\tau_{b1} = 0.328229581037703$
$\tau_{c2} = 127.987122286458$	$\tau_{b2} = 0.116382150788257$
$\tau_{c3} = 36.4498035498791$	$\tau_{b3} = 0.170088689025220$
$\tau_{c4} = 0.431601172583449$	$\alpha_1 = -0.852875777762097$
$\beta_1 = -0.295752216445804$	$\alpha_2 = 0.355985006341193$
$\beta_2 = -0.209472496072177$	$\alpha_3 = 0.09024721408496$
$\beta_3 = -1.45128957397682$	$\lambda_{x0} = -0.120886982074471$
$\lambda_{y0} = 0.112474559675909$	$\lambda_{z0} = 0.194220406349215$
$\lambda_{Vx0} = 0.152137708649055$	$\lambda_{Vy0} = 0.012783664381524$
$\lambda_{Vz0} = -0.240807211082437$	

and 1836.70 kg, respectively, with the total fuel consumption 6637.83 kg. There is a minimal 5.2 kg difference in fuel consumption (0.8%). Since the thrust-to-mass ratio is high and the burn arcs are relatively short, the optimal solution with inertially fixed model can be very close to the optimal solution with freely steering thrust. Such a small performance loss seems acceptable, and inertially-fixed steering appears to be preferable when its simplicity is taken into account for a spacecraft with a comparably high thrust-to-mass ratio. The additional fuel consumption mainly appears in the first burn, as the transfer arc of the first burn is the longest. As expected, the linear varying thrust model results in lower fuel cost, and almost exactly matches the optimal solution using unconstrained thrust direction. The indirect optimizer converges very quickly in terms of CPU time of an ordinary PC (in minutes).

As already mentioned, the thrust structure is specified a priori in order to guarantee precise integration, and the optimality of the solution obtained can be verified by checking the switching function. Figure 2 and Figure 3, respectively, show the thrust and its associated switching function S_F for the two steering thrust models, as given by Eq.(32) and Eq.(56), respectively. It can be observed that the necessary conditions arising from the PMP are satisfied correctly. Although the switching function curves for both cases remain close to

Table 2: Fuel consumption (kg) comparison for different steering models (main engine case).

Steering model	Free	Inertially fixed	Linearly varying
Burn 1	3538.05399	3544.38	3538.05401
Burn 2	1257.28628	1256.75	1257.28634
Burn 3	1837.31379	1836.70	1837.31378
Total burns	6632.65406	6637.83	6632.65413

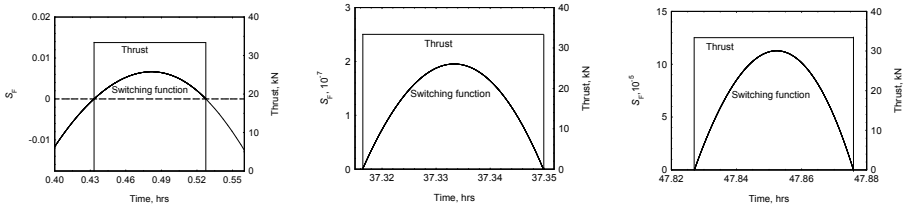

(a) first burn (b) second burn (c) third burn

Figure 2: Switching function for inertially fixed thrust(case 1)

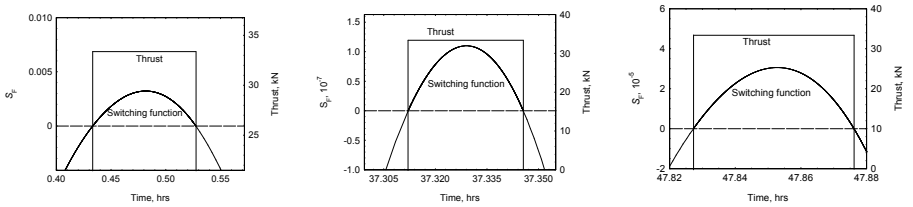

(a) first burn (b) second burn (c) third burn

Figure 3: Switching function for linearly varying thrust (case 1)

zero during the second burn, which has the task of performing the plane change and velocity increase, they behave regularly and stay consistently positive, as shown in Figure 2(b) and Figure 3(b). Similar behaviors are also found during the third burn, as shown in Figure 2(c) and Figure 3(c). It is important to note that in the solution obtained by Yan et al. [7] a singular arc constitutes the second burn; however, the analysis of the switching function and the better results obtained in previous work [9] show that all the controls should be bang-bang.

Figure 4 displays the position and velocity of the optimal trajectory, which exhibits four coast arcs separated by three burns. The first coast arc is introduced to move on the parking orbit until the most favorable phase angle before departure is reached. The first burn at periapsis raises apoapsis to about 30,000km; the second burn has the main task of changing the orbit plane after crossing the apoapsis, but it also increases the orbit energy; finally, the third burn accelerates the spacecraft to arrive at the desired escape state.

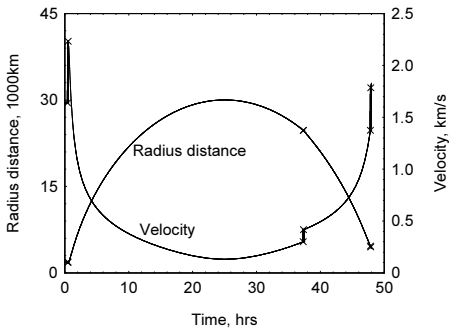

Figure 4: Position and velocity of the optimal trajectory for the thrust with constant steering rate (case 1), bold lines indicate thrust arcs

Table 3: Comparison between inertially fixed and fixed-plane linearly varying steering models (main engine case).

Results	Duration, s	Linear steering Thrust rotation rate, deg/s	Total thrust rotation, deg	Inertially fixed Duration, s
burn 1	339.04	3.637e-2	12.33	339.65
burn 2	120.48	4.826e-4	0.06	120.43
burn 3	176.07	9.753e-3	1.72	176.01

Table 4: Fuel consumption (kg) comparison for different steering models (auxiliary engine case).

Steering model	Free	Inertially fixed	Linearly varying
Burn 1	3998.12	4671.22	4002.52
Burn 2	1265.22	1300.94	1265.74
Burn 3	1901.63	1737.22	1900.91
Total burns	7164.98	7709.37	7169.17

Table 3 shows the amount of thrust vector rotation required for the fixed-plane linear steering model to outperform the inertially fixed steering model. It can be seen that the first and third burns require the greatest thrust vector rotation, while the second burn benefits very little from the ability to steer the thrust vector. The second burn is not only very short, but also its thrust vector tends to point along a fixed inertial direction, with only 4.826e-4 deg/s steering rate and hence results in only 0.06deg rotation. This fact is also reported by Ocampo and Muthur [1]. This is expected, since the second burn in such a three-burn sequence is a relatively short-duration plane-change maneuver, so the optimal thrust direction is nearly fixed and perpendicular to the orbit plane. On the other hand, the direction is not absolutely fixed, but rather rotates very slowly.

5.2. Case 2: auxiliary engine of the Orion

The Orion auxiliary engine is associated with different steering models. The optimal flight time is again at the limiting value of 48 hours. Table 4 shows the results of fuel consumption for different steering models, from which it can be seen that reducing the thrust increases the difference between inertially fixed and linearly varying thrust models. As a reference solution, the fuel consumptions of the optimal trajectory with freely varying thrust is 3998.12 kg, 1265.22 kg, and 1901.63 kg for first, second and the third burn, respectively, with total fuel consumption of 7164.98 kg. The lower specific impulse results in 532.3 kg more fuel in comparison to case 1.

For an inertially fixed thrust model, the fuel consumption for the first, second, and third burn is 4671.22, 1300.94, and 1737.22 kg, respectively, with the

Table 5: Comparison between inertially fixed and fixed-plane linearly varying steering models (auxiliary engine case).

Results	Duration, s	Linear steering Thrust rotation rate, deg/s	Total thrust rotation, deg	Inertially fixed Duration, s
burn 1	2723.77	3.256e-2	88.78	3182.32
burn 2	861.95	4.620e-4	0.38	886.28
burn 3	1295.51	9.564e-3	12.39	1183.50

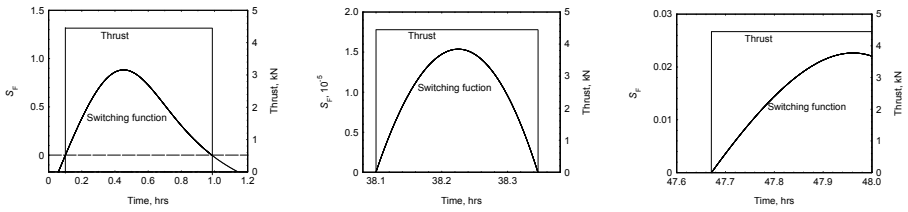

(a) first burn (b) second burn (c) third burn

Figure 5: Switching function for inertially fixed thrust(case 2)

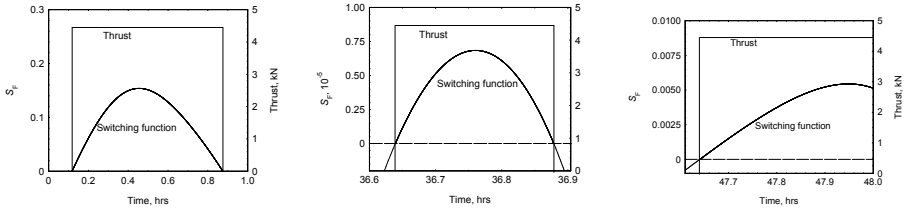

(a) first burn (b) second burn (c) third burn

Figure 6: Switching function for linearly varying thrust(case 2)

total fuel consumption of 7709.37 kg. The difference with respect to the free-steering solution for Case 2 is a total of 544.4 kg, or 7.6 % more fuel used. Since the thrust-to-mass ratio is small, the optimal solution with the inertially fixed model diverges noticeably from the optimal solution with free thrust. In contrast, the benefit of the linear steering model becomes immediately apparent, which results in a significant fuel reduction compared with that of the inertially fixed model. The solution is again very close to the optimal one, as a linear change in thrust direction quite accurately follows the reference free-steering solution. Similar to the previous case, all the burns appear to require full thrust (see Figure 5 and Figure 6), in agreement with PMP, and singular arcs do not seem to be needed.

Figure 5(b) shows that the switching function behaves regularly and remains consistently positive during the burn. The rotation span of the second burn is enlarged to 0.38 deg using constant steering rate of 4.620e-4 deg/s, due to the lower available thrust, see Table 5. According to the optimal trajectory, shown in Figure 7, the control structure includes 6 arcs. In comparison to case 1, the first coast arc becomes very short and the final coast arc disappears. The lower thrust level requires longer burns, and the behavior of the thrust angles becomes more complex; however, the thrust vector of the second burn tends again to be inertially fixed.

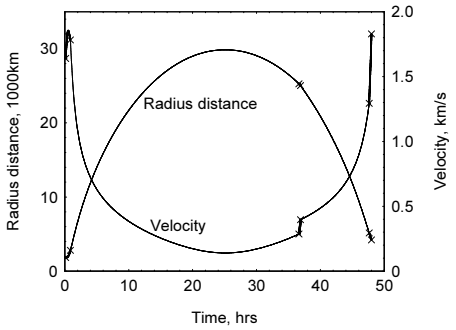

Figure 7: Position and velocity of the optimal trajectory for the thrust with constant steering rate (case 2), bold lines indicate thrust arcs

6. Conclusions

Indirect optimization methods are usually considered to be not suited to problems with complex dynamics and constraints. In this paper, an indirect method is developed to model high-accuracy finite-burn optimal trajectories, where two different finite-burn maneuver steering models are introduced to take practical limitations of the spacecraft steering capabilities into account. The first is an inertially fixed model, in which the thrust direction is fixed during each burn arc. The second is a fixed-plane linear steering model, in which the thrust direction is allowed to rotate at a constant rate about a rotation axis for each finite-burn maneuver. Conditions for optimality are derived and the arising boundary value problem is solved numerically.

The developed numerical optimization procedure has been used to find the optimal strategies of Moon-escape trajectories of a spacecraft with a realistic steering and thrust model. The total propellant mass for the transfer from a low lunar parking orbit to specified escape conditions is minimized. The problems dealt with in this article show that the proposed approach can be profitably used for the analysis of practical finite-burn transfers. The proposed indirect method is simple and relatively fast, and provides high-accuracy flyable solutions; convergence difficulties are easily solved by means of continuation techniques. Therefore this optimization procedure combines accuracy, robustness, and speed and constitutes a powerful tool for trajectory analysis in a complex dynamical environment using practical controls.

As expected, results show that optimized solutions with inertially-fixed thrust are close to the freely steering solutions when the thrust-to-mass ratio is relatively high, whereas the linear steering model can provide notable benefit over the inertially-fixed model when thrust-to-mass ratio is instead low. Results also show that the switching function of the optimal solutions has a regular behavior

and suggests the use of a bang-bang control. This precise satisfaction of PMP comes from the intrinsically higher accuracy of indirect methods compared to other methods commonly employed.

Acknowledgments

This research was partially supported by the National Natural Science Fund No. 11702330, U1713223 and 61673026.

References

[1] Ocampo, C. A., and Mathur, R., "Variational Model for Optimization of Finite-Burn Escape Trajectories Using a Direct Method," Journal of Guidance, Control, and Dynamics, 35, No. 2 (2012) 598-608. doi:10.2514/1.46955

[2] Jones, D. R., and Ocampo, C., "Optimization of Impulsive Trajectories from Circular Oribt to an Excess Velocity Vector," Journal of Guidance, Control, and Dynamics, 35, No. 1 (2012) 234-244. doi: 10.2514/1.49237

[3] Ocampo, C., and Saudemont, R., "Initial Trajectory Model for a Multi-Maneuver Moon-to-Earth Abort Sequence," Journal of Guidance, Control, and Dynamics, Vol. 33, No. 4, (2010) 1184-1194. doi:10.2514/1.46955

[4] Shen, H.-X., Zhou, J.-P., Peng, Q.-B., and Li, H.-Y., "Point Return Orbit Design and Characteristics Analysis for Manned Lunar Mission," Science China Technological Sciences, 55, No. 9 (2012) pp. 2561-2569. doi: 10.1007/s11431-012-4969-4

[5] Shen, H. -X., Casalino, L., "Indirect Optimization of Three-Dimensional Multiple-Impulse Moon-to-Earth Transfers," The Journal of Astronautical Sciences, 61 (2014) 255-274. doi: 10.1007/s40295-014-0018-9

[6] Edelbaum, T. N., "Optimal Nonplanar Escape from Circular Orbits," AIAA Journal, 9, No. 12 (1971) 2432-2436. doi:10.2514/3.50047

[7] Yan, H., Gong, Q., Park, C., and Ross, I. M., "High-Accuracy Trajectory Optimization for a Trans-Earth Lunar Mission," Journal of Guidance, Control, and Dynamics, 34, No. 4 (2011) 1219-1227. doi: 10.2514/6.2010-7726

[8] Park, C., "Necessary Conditions for the Optimality of Singular Arcs of Spacecraft Trajectories Subject to Multiple Gravitational Bodies," Advances in Space Research, 51 (2011) 2125-2135. doi:10.1016/j.asr.2013.01.005

[9] Shen, H. -X., Casalino, L., "High-accuracy optimal finite-thrust trajectories for Moon escape," Acta Astronautica, 131 (2017) 102-109. doi: 10.1016/j.actaastro.2016.11.028

[10] Colasurdo, G., and Casalino, L., "Indirect Methods for the Optimization of Spacecraft Trajectories," in: Fasano, G, Pinter J.P. (Eds.), Modeling and Optimization in Space Engineering, Springer, New York Heidelberg Dordrecht London, 2012, pp. 141-158.

[11] Bertrand, R., and Epenoy, R., "New smoothing techniques for solving bang–bang optimal control problems—numerical results and statistical interpretation," Optimal Control Applications and Methods 23, No. 4 (2002) 171-197. doi: 10.1002/oca.709.

[12] Haberkorn, T., Martinon, P., and Gergaud, J., "Low thrust minimum-fuel orbital transfer: a homotopic approach," Journal of Guidance, Control, and Dynamics 27, No. 6 (2004) 1046-1060. doi: 10.2514/1.4022.

[13] Jiang, F., Baoyin, X., and Li, J.. "Practical techniques for low-thrust trajectory optimization with homotopic approach," Journal of Guidance, Control, and Dynamics 35, No. 1 (2012) 245-258. doi: 10.2514/1.52476.

[14] Pan, B., Lu, P., Pan, X., and Ma, Y., "Double-homotopy method for solving optimal control problems," Journal of Guidance, Control, and Dynamics 39, No. 8 (2016): 1706-1720. doi: 10.2514/1.G001553.

[15] Taheri, E., Kolmanovsky, I., and Atkins, E., "Enhanced smoothing technique for indirect optimization of minimum-fuel low-thrust trajectories," Journal of Guidance, Control, and Dynamics 39, No. 11 (2016) 2500-2511. doi: 10.2514/1.G000379.

[16] Zhu, Z., Gan, Q., Yang, X., and Gao, Y., "Solving fuel-optimal low-thrust orbital transfers with bang-bang control using a novel continuation technique," Acta Astronautica 137 (2017): 98-113. doi: 10.1016/j.actaastro.2017.03.032.

[17] Bryson, A. E., and Ho, Y.-C., Applied Optimal Control, rev. ed., Hemisphere, Washington, DC, 1975, pp. 42-89.

[18] Casalino, L., Colasurdo, G., and Pastrone, D., "Optimal Low-Thrust Escape Trajectories Using Gravity Assist," Journal of Guidance, Control, and Dynamics, 22, No. 5 (1999) 637-642. doi: 10.2514/2.4451

[19] Lawden, D. F., Optimal Trajectories for Space Navigation, Butterworths, London, 1963.

[20] Casalino, L., "Singular Arcs During Aerocruise," Journal of Guidance, Control, and Dynamics, 23, No. 1 (2000) 118-123. doi: 10.2514/2.4494

[21] Shen, H. -X., Casalino, L., and Li, H.-Y. "Adjoints Estimation Methods for Impulsive Moon-to-Earth Trajectories in the Restricted Three-Body Problem," Optimal Control Applications and Methods, 36 (2015) 463-474. doi: 10.1002/oca.2120

[22] Colasurdo, G., and Pastrone, D., "Indirect Optimization Method for Impulsive Transfer," AIAA Paper 1994-3762, 1994.